Chiral Electronic Transitions in Fluorescent Silver Clusters Stabilized by DNA

Steven M. Swasey,[†] Natalia Karimova,[‡] Christine M. Aikens,[‡] Danielle E. Schultz,[†] Anna J. Simon,[†] and Elisabeth G. Gwinn[§,*]

[†]Department of Chemistry and Biochemistry, University of California, Santa Barbara, Santa Barbara, California 93106, United States, [‡]Department of Chemistry, Kansas State University, Manhattan, Kansas 66506, United States, and [§]Department of Physics, University of California, Santa Barbara, Santa Barbara, California 93106, United States

ABSTRACT Fluorescent, DNA-stabilized silver clusters are receiving much attention for sequence-selected colors and high quantum yields. However, limited knowledge of cluster structure is constraining further development of these "Ag_N-DNA" nanomaterials. We report the structurally sensitive, chiroptical activity of four pure Ag_N-DNA with wide ranging colors. Ubiquitous features in circular dichroism (CD) spectra include a positive dichroic peak overlying the lowest energy absorbance peak and highly anisotropic, negative dichroic peaks at energies well below DNA transitions. Quantum chemical calculations for bare chains of silver atoms with nonplanar curvature also exhibit these striking features, indicating electron flow along a chiral, filamentary metallic path as the origin for low-energy Ag_N-DNA transitions. Relative to the bare DNA, marked UV changes in CD spectra of Ag_N-DNA and silver cation−DNA solutions indicate that ionic silver content constrains nucleobase conformation. Changes in solvent composition alone can reorganize cluster structure, reconfiguring chiroptical properties and fluorescence.

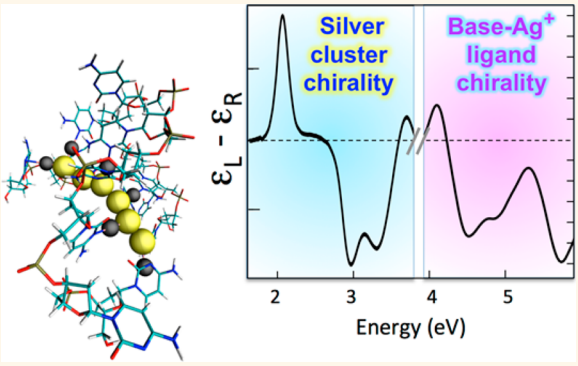

KEYWORDS: fluorescent silver clusters · circular dichroism · anisotropy · time-dependent density functional theory · DNA-templated clusters · Ag-DNA

Advances in chemical control over the shape, as well as size, of metal nanoparticles are resulting in remarkable optical signatures of chirality.[1−8] Recent studies found that decorating 50 nm metal nanoparticles with DNA could lead to circular dichroism (CD) signals at visible wavelengths spanning the plasmonic response of the metal particles.[1] This visible signature of induced chirality occurred at energies 1−2 eV below the ultraviolet (UV) CD of DNA itself, which arises in the 4−6 eV range (200−300 nm) from differences in the absorption of left and right circularly polarized light that characterize the specific chiral arrangement of the bases. The visible CD enhancement *via* coupling of plasmonic absorption to UV transitions of DNA was greatly increased by use of nonspheroidal metal nanoparticles, pointing to the crucial role of metal particle shape.

At the much smaller (∼1 nm) size scale of metal clusters, optical signatures of chirality are also evident and are particularly exciting due to the emergence of strong fluorescence in the cluster size regime. Gold and silver clusters protected by chiral ligand monolayers exhibit circular dichroism near wavelengths of metal-based transitions.[2,3] Intrinsically chiral ligands are not even necessary for cluster chirality. $Au_{38}(SR)_{24}$ clusters with achiral thiol ligands displayed pronounced CD signals,[4,5] reflecting a chiral pattern of ligand attachment that shapes a chiral metal cluster.[3]

While a chiral twist in cluster shape, and thereby on free electron currents, should be easier to impress on elongated rather than spherical clusters, effects of the shape of gold clusters on the chirality of electronic transitions are not well understood. Interpretation of the chiroptical properties is

* Address correspondence to bgwinn@physics.ucsb.edu.

Received for review March 23, 2014 and accepted June 4, 2014.

Published online June 04, 2014
10.1021/nn5016067

TABLE 1. Ag_N-DNA Properties

ID	template strand	exc.[a] energy	emission energy[a]	Ag^{0}[b]	Ag^{+}[b]
S1	CCCACCCACCCGCCCA	1.74 eV (711 nm)	1.60 eV (776 nm)	12	8 or 9
S2	GGCAGGTTGGGGTGACTAAAAACCCTTAATCCCC	2.06 eV (601 nm)	1.83 eV (677 nm)	6	9
S3	CACCGCTTTTGCCTTTTGGGGACGGATA	2.07 eV (600 nm)	1.85 eV (670 nm)	6 or 7	8 or 9
S4	TGCCTTTTGGGGACGGATA	2.55 eV (487 nm)	2.19 eV (566 nm)	4	6

[a] Aqueous visible fluorescence excitation maxima and emission maxima. [b] Numbers of neutral silver atoms (Ag^0) and numbers of silver cations (Ag^+) in the Ag_N-DNA templated by the indicated strand. Reported values from refs 18 and 19 were determined by mass spectrometry of the pure Ag_N-DNA in ~30% methanol solvent.

complicated by the broad band of transitions arising from d orbitals of gold, which spread across the range of the shape-dependent cluster excitations and into the UV. Although silver nanoparticles[6,9] and clusters[10−16] are less studied than their gold counterparts, silver has the advantage of weaker, higher energy d-band transitions. Thus, silver-based particles have potential for strong chiral signatures with a transparent relation to cluster structure and associated promise for use in chiral-sensing applications.

Recently it was shown that silver clusters with sizes of 10−20 silver atoms, stabilized by DNA, can be isolated with compositional purity.[17,18] Optical studies of pure, fluorescent Ag_N-DNA, which contain cationic as well as neutral silver atoms, suggested a rod-like structure for a neutral silver cluster core, with core length governing color.[19,20] If chiral, such elongated clusters might be expected to exhibit particularly rich CD signatures.

Here we investigate the chirality of the optical transitions in pure Ag_N-DNA with cluster emission colors ranging from blue-green through the near-infrared (Table 1). Samples S2 and S3 are stabilized by different DNA template strands but hold silver clusters with similar absorbance and emission spectra. Previous studies[18,19] identified the composition of S2[21] and S3 as six to seven silver atoms in the neutral cluster core, with eight to nine silver cations also incorporated into the Ag_N-DNAs. The red-shifted emitter S1[22] contains 12 neutral silver atoms in the cluster core and eight to nine silver cations,[18,19] while the blue-shifted emitter S4 holds four neutral silver atoms in the core and six silver cations. This selection of Ag_N-DNA probes the chirality of visible through IR absorbance transitions that correspond to peak excitation of fluorescence. In the UV, changes in CD relative to the bare DNA template strands indicate nucleobase rearrangement by cluster−DNA interactions. While early studies of DNA-stabilized silver clusters also investigated UV chirality using CD spectroscopy, these investigations used unpurified solutions,[23−25] which typically contain mixtures of many different silver−DNA products and consequently cannot address chirality of specific DNA-stabilized silver clusters.

RESULTS

Reshaping of UV Circular Dichroism in Ag_N-DNA. In native DNA, chiroptical activity in the 4.1−6.2 eV range (200−300 nm) arises largely from the relative orientations of transition dipoles of the chromophoric bases and therefore is extremely sensitive to conformational changes. To investigate the effects of the strand-embedded silver clusters on the shaping of the DNA itself, we compare the UV circular dichroism of the bare DNA strands, the nonfluorescent solutions of the DNA strands incubated with unreduced silver ions (Ag^+-DNA), and the purified fluorescent Ag_N-DNA solutions (Figure 1). The Ag^+-DNA solutions had the same $[Ag^+]/[DNA]$ as used in synthesis of the pure Ag_N-DNA (SI).

The bare DNA strands (black curves, Figure 1a−d) show a positive CD peak near 4.5 eV (270−280 nm) and a negative peak near 5.0 eV (250 nm), as expected for random coil DNA.[26−28] The attachment of Ag^+ (Ag(I) cations) to the DNA produces large negative CD features (red curves, Figure 1a−d). In contrast to the large changes in CD spectra, the UV absorbance spectra are similar in the absence/presence of either Ag^+ or the pure clusters (Figure 1e). We attribute the Ag^+-induced reorganization of the UV CD to the known ability of silver cations to mediate artificial base-pairing,[29−32] which should alter relative orientations of base transition moments and change UV CD relative to the bare DNA.

The blue curves in Figure 1a−d show the UV CD spectra of the pure, fluorescent cluster solutions. In all cases the striking, negative CD bands are quite distinct from the bare DNA spectra and overall more similar to the UV CD spectra of the DNA-Ag^+ solutions. (For the *im*pure reduced solutions, which contain many different species of Ag-bearing DNA, CD amplitudes are reduced and additional weak peaks appear (SI).)

The CD anisotropy, or dissymmetry, $g = (A_L - A_R)/A = \Delta\varepsilon/\varepsilon$, provides a useful dimensionless measure of the chirality of electronic transitions[33] (A_L and A_R are absorbances for left and right circularly polarized light). All of the pure Ag_N-DNA samples show prominent, negative CD peaks near 4.7 eV, with g values of -1×10^{-3} to -2.3×10^{-3}, and near 5.7 eV, with g values of -3×10^{-3} to -6×10^{-3} (Table 2 gives experimental g values at the energies of individual fitted Gaussian CD peaks, discussed below). These values are up to ~30 times larger than for the bare DNA and point to the persistence of silver-mediated base-pairing in the pure Ag_N-DNA. Such pairing should constrain relative

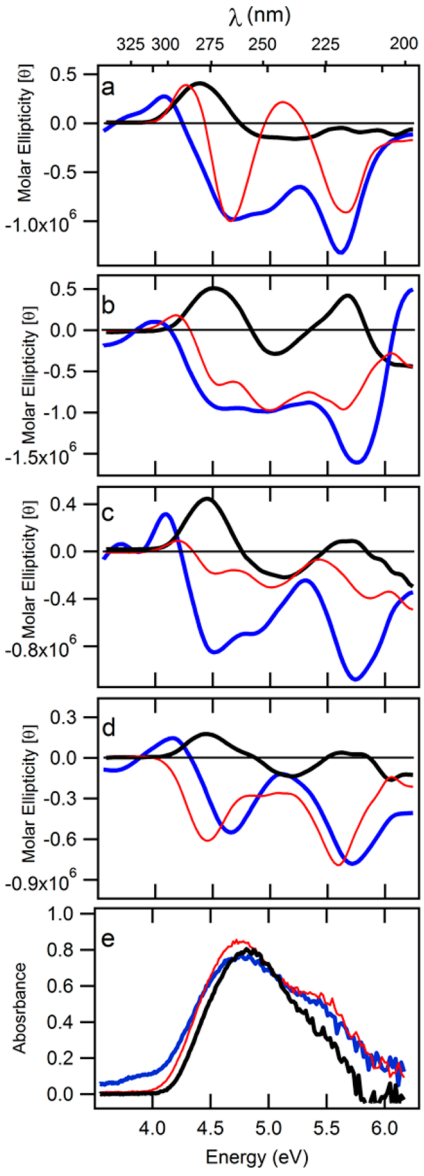

Figure 1. (a–d) UV CD spectra for templates S1–S4, respectively. Black curves are bare DNA template solutions, red curves are DNA-Ag^+ solutions, and blue curves are the pure cluster solutions. In all cases, DNA-Ag^+ interactions produce negative-going CD, which is further enhanced in the pure cluster solutions. (e) Absorbance spectra of the S3 template strand (black), S3 template with Ag^+ (red), and the pure S3 Ag_N-DNA (blue).

nucleobase orientations more than in random coil DNA, enhancing CD by reducing fluctuational averaging. Apparently the formation of the neutral silver clusters leaves intact much of the DNA structuring produced by Ag^+-mediated base interactions in the Ag^+-DNA solutions. This is consistent with the simultaneous presence of silver cations and neutral silver atoms in the pure Ag_N-DNA (Table 1) and with incorporation of silver clusters *via* base–Ag^+-silver cluster bonding, as previously suggested.[19]

The UV peaks in the Ag_N-DNA CD spectra might instead arise from high-energy transitions of the clusters themselves, rather than from the base chromophores. However, the overall similarity of the pure Ag_N-DNA CD spectra and the CD spectra of the unreduced Ag^+-DNA solutions, which cannot contain clusters of metallically bonded silver atoms, suggests that the DNA plays the dominant role in the UV chirality.

Low-Energy, Cluster-Dominated CD. We now turn to the CD features induced at low energies by the incorporation of silver clusters into the templating DNA strands (black curves, Figure 2). Comparison to absorbance spectra of the pure cluster solutions (blue curves, Figure 2) shows that in all cases a positive dichroic peak overlies the low-energy cluster absorbance transition, which itself lies at energies well below the d-band transitions in silver. Because the absorbance peak coincides with peak fluorescence excitation,[34] we tested the possibility that the CD signal might be spurious polarized light emission by using a short-pass filter to block the fluorescence from entering the detector. The negligible change in the CD signal confirmed that it originates from differential absorbance of left and right circularly polarized light.

This striking *mono*signate CD signal (Figure 2, red stars) differs qualitatively from the *bi*signate excitonic splittings characteristic of macromolecular CD spectra, which arise in the UV from dipolar couplings of the transition moments of the chromophores. Bisignate CD also results from coupling of the plasmonic dipole moments of disconnected, spherical metal nanoparticles that are arranged in chiral patterns. In such multinanoparticle assemblies, the positive–negative bisignate peaks lie near the plasmon energy of the individual particles.[7] If an Ag_N-DNA contained multiple smaller clusters, rather than a single connected cluster, dipolar intercluster couplings would also be expected to produce bisignate CD, though such effects should be greatly weakened relative to the case of ~10 nm coupled nanoparticles due to the much smaller number of free electrons in the cluster limit.

The monosignate form of the CD signal in Figure 2 and its transparent association with a cluster-centered absorbance transition also differ strikingly from the chiroptical signatures of ligand-protected gold clusters with similar numbers of metal atoms.[5] In such Au clusters, there is no well-resolved absorbance peak that can be identified with a collective excitation of delocalized electrons in the cluster. Instead the broad absorbance spectrum extends from the UV through ~800 nm and the corresponding CD signal oscillates rapidly in sign. Here, in contrast, the absorbance shows a distinct low-energy peak and the CD signal exhibits the same shape (Figure 2, red stars). These features strongly suggest that electronic chirality of this transition reflects a continuous, chiral metal path for free electrons.

Giant Anisotropies at Intermediate Energies. Below 4 eV, neither the bare DNA nor the Ag^+-DNA solutions show

TABLE 2. Experimental Anisotropy Values ($g \times 10^3$) at Energies of Individual Fitted Gaussian CD Peaks (eV)

peak	S1	S2	S3	S4
1	0.305 ± 0.001	0.37 ± 0.01	0.753 ± 0.002	0.389 ± 0.001
	(1.76 eV)	(2.09 eV)	(2.07 eV)	(2.54 eV)
2	−9.2 ± 0.3	−29 ± 13	−6.7 ± 0.1	−6.4 ± 0.2
	(3.16 eV)	(3.19 eV)	(2.98 eV)	(3.29 eV)
3	−5.9 ± 0.1	−11 ± 2	−6.3 ± 0.1	−2.33 ± 0.04
	(3.42 eV)	(3.55 eV)	(3.32 eV)	(3.68 eV)
4	3.84 ± 0.02	0.045 ± 0.005	1.50 ± 0.01	0.849 ± 0.004
	(4.09 eV)	(4.13 eV)	(4.12 eV)	(4.18 eV)
5	−2.33 ± 0.01	−1.30 ± 0.06	−1.268 ± 0.002	−0.986 ± 0.001
(UV)	(4.66 eV)	(4.35 eV)	(4.47 eV)	(4.66 eV)
6	−2.12 ± 0.01	−1.04 ± 0.02	−0.850 ± 0.001	−0.364 ± 0.001
(UV)	(5.08 eV)	(5.06 eV)	(4.89 eV)	(5.21 eV)
7	−5.9 ± 0.01	−3.3 ± 0.2	−3.47 ± 0.01	−3.000 ± 0.008
(UV)	(5.62 eV)	(5.78 eV)	(5.75 eV)	(5.73 eV)

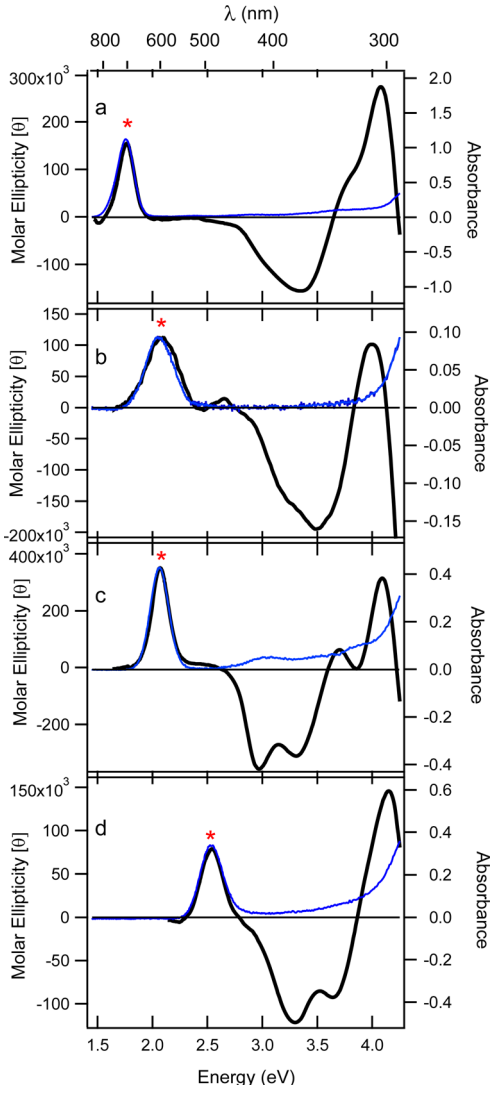

Figure 2. CD (black) and absorption (blue) spectra of pure cluster solutions S1 (a), S2 (b), S3 (c) (aqueous solution), and S4 (d; 50% MeOH). A positive CD peak overlies the collective longitudinal cluster absorbance peak (red stars).

a CD signal. Thus, all CD features at energies below 4 eV are due to the free electrons from the neutral silver atoms in Ag_N-DNA, which are also responsible for fluorescence. Figure 2 shows that although the absorbance between the low-energy peak and the UV region is quite weak, the presence of clusters induces very pronounced CD features with negative anisotropies and high g, reaching *ca.* -10×10^{-3} (Table 2), similar to the largest magnitudes of g reported for chiral, thiol-protected gold clusters.[5]

Fits to CD Spectra. Across the entire spectral range, fits to the superposition of seven dichroic peaks with Gaussian line shapes (SI) give consistent results for signs and strengths of the CD spectra of the pure Ag_N-DNA (Figure 3). The similar energies and amplitudes of the fitted peaks (SI; Table 2 gives peak energies) again indicate that the silver−silver and cluster−base bonding are similar for all four cluster species, despite their quite different DNA template strands (Table 1). Thus, the geometry of the silver cluster is the primary determinant of the optical response, rather than detailed strand composition. It appears that particular base motifs are selecting the cluster geometry and that distinct base motifs can produce the same cluster structure.

Quantum Chemical Calculations. Previous experimental studies of pure Ag_N-DNA found evidence for an elongated, rod-like cluster structure in which the low-energy absorbance resonance arises from the longitudinal collective response of the cluster's free electrons.[19] Nonplanar curvature of such a filamentary cluster would result in chiral currents and circular dichroism. The consistently positive sign of the lowest energy CD peak would then be associated with the flow of free electrons along clusters with consistent helicity across the 4−12 atom neutral cluster sizes in samples S1−S4, in qualitative agreement with their similar anisotropy values, $g = 0.3 \times 10^{-3}$ to $g = 0.75 \times 10^{-3}$.

To investigate whether chiral, filamentary silver clusters in the several atom size range could exhibit chiroptical properties similar to Ag_N-DNA, we used

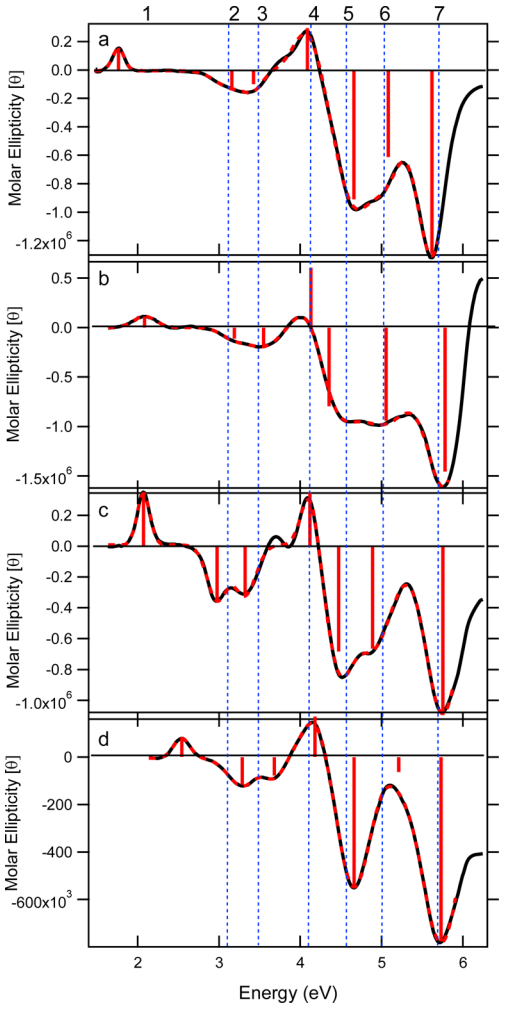

Figure 3. Fits (red dashed curves) of experimental CD spectra (black curves) to the superposition of seven Gaussian peaks for S1 (a), S2 (b), S3 (c) (aqueous solution), and S4 (d) (50% MeOH). Peaks are numbered; 1 represents the lowest energy peak for each spectrum (no guideline shown). Red bars: fitted amplitudes, at fitted energies (fit parameters are tabulated in the SI).

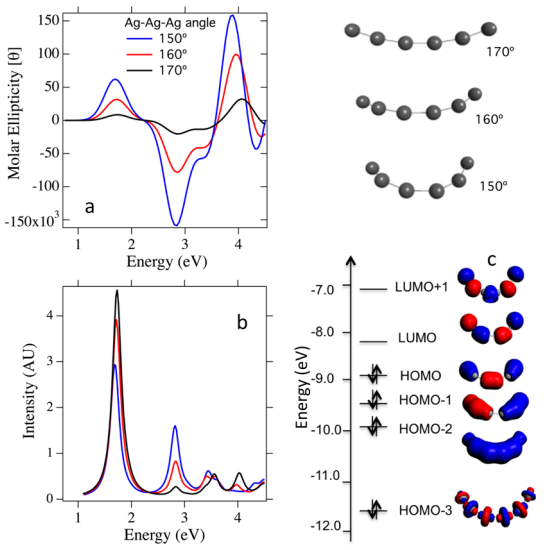

Figure 4. Calculated circular dichroism spectra (a) and optical absorption spectra (b) for neutral, filamentary Ag_6 clusters shown at the top right. Calculations use the SAOP functional with the TZP basis set. (c) Kohn–Sham orbitals and energies for the 150° Ag–Ag–Ag angle and 10° torsional angle.

time-dependent density functional theory to calculate absorbance and CD spectra of six-atom neutral silver cluster chains with nonplanar curvature (Figure 4). Cluster shapes were selected to have a simple chiral form, a filamentary shape with 170°, 160°, and 150° Ag–Ag–Ag bond angles, a 2.7 Å bond length, and a torsional (dihedral) Ag–Ag–Ag–Ag angle of 10°. (For a torsional angle of 0°, the clusters are achiral, with increasing planar curvature for decreasing Ag–Ag–Ag angles below 180°.)

Overall, the calculated spectra in Figure 4 are strikingly similar to the data (Figure 2 and Figure 3 below ~4.5 eV; DNA transitions dominate at higher energy). The lowest energy calculated CD peak is positive (Figure 4a) and overlies the lowest energy absorbance transition (Figure 4b). In terms of molecular orbitals (Figure 4c), this is a HOMO–LUMO transition, corresponding to the collective, phased oscillation of all the cluster electrons. At higher energies, the calculated CD exhibits pronounced negative peaks, as in the data. These arise from HOMO → LUMO+1, HOMO−1 → LUMO, and HOMO−3 → LUMO transitions that are forbidden in perfectly straight wires. (The HOMO–LUMO gap for all structures is 0.7 eV.)

The lowest energy, positive CD peak for all calculated structures appears near 1.7 eV, with negative dichroic peaks near 2.8 and 3.3 eV (Figure 4a). This is in good agreement with the data for sample S2, which has the same neutral silver content (six atoms), a positive CD peak at 2.0 eV, and first and second negative CD peaks at 3.0 and 3.3 eV. While peak energies agree rather well between calculation and experiment (within ~0.3 eV), this may be partly fortuitous for the lowest energy transition. The energy of these longitudinal plasmon-like excitations is expected to increase with decreasing Ag–Ag–Ag angle within the cluster[35] and to decrease with increasing refractive index of the medium (vacuum for the calculations). To the extent that these effects do not cancel, the lowest energy peak will shift.

In the calculated CD, peak energies and relative peak amplitudes depend only weakly on the Ag–Ag–Ag angle, but the CD intensity rises rapidly as decreasing the Ag–Ag–Ag angle increases chirality (Figure 4a). Below 4 eV, the integrated CD peak intensities for sample S2 are similar to the calculated CD for a 150° Ag–Ag–Ag angle and 10° torsional angle. (Above ~4 eV, bare cluster calculations are not comparable to data because the DNA dominates the high-energy CD spectra of Ag_N-DNA.) The ratio of integrated spectral weights in calculation *versus* experiment

is ~0.8 for the positive dichroic peak as well as for the negative dichroic peaks.

In contrast to the insensitivity of the spectral shapes in calculated CD spectra to the Ag−Ag−Ag angle, the calculated absorbance spectra show a marked increase in the relative intensity of the peak near 3 eV as the Ag−Ag−Ag angle decreases from 170° to 150° (Figure 4b). The rise of this absorbance peak corresponds to a large increase in the overall CD intensity (Figure 4a). The behavior of calculated CD and absorbance is consistent with the differences in CD and absorbance spectra of sample S3 relative to sample S2. Sample S3 has larger absorbance near 3 eV than sample S2 (Figure 2b,c, blue traces), which according to the calculations implies higher chirality in S3 than in S2. Consistent with this expectation, the integrated CD peak strengths in sample S3 are 2 times larger than in sample S2 (Figure 2b,c, black curves). While only sample S3 exhibits a resolved absorbance peak near 3 eV, the similar pronounced, negative features in the CD of samples S1, S2, and S4 indicate that such an absorbance transition is weakly present but obscured by the noise in the absorbance signal.

In order to understand how peak locations and peak amplitudes depend on the torsional angle, as opposed to the Ag−Ag−Ag angle investigated in Figure 4, we calculated structures with a fixed Ag−Ag−Ag angle of 160° and different torsional angles from 10° to 60°. The calculated CD spectra show that the absolute peak locations are insensitive to the torsional angle, whereas the peak amplitudes initially rise rapidly with increasing torsional angle and saturate at a torsional (Ag−Ag−Ag−Ag) angle of ~50°. The low-energy, positive dichroic peak and the negative dichroic peak at 2.8 eV are roughly 3 times more intense at a helical angle of 50° than 10°. Apparently differences in torsional angle could account for the difference in CD intensities for same-size clusters measured in experiment.

To examine the length dependence of the optical absorption and CD of these filamentary wires, TDDFT calculations were performed on Ag_n (n = 4, 6, 8, 10, 12) clusters with 170° Ag−Ag−Ag bond angles and a 10° torsional (dihedral) Ag−Ag−Ag−Ag angle. For n values from 4 to 8, the absorption shows only one strong peak, which linearly shifts to lower energy with increasing n, while the longer systems exhibit an additional, weaker but significant peak at ~1 eV higher energy than the dominant low-energy transition (Figure SI.3A). CD spectra (Figure SI3.B) also become stronger and red-shift as n increases. For all n the CD exhibits a strong, monosignate, positive first peak coinciding with the main absorbance peak (the HOMO−LUMO transition), as in the data. For all n the second dichroic peak has a negative sign, also in qualitative agreement with the data. As discussed for Ag_6, this peak arises from the HOMO → LUMO+1 and HOMO−1 → LUMO transitions that are forbidden for perfectly linear wires. In all cases this second peak is strong in the CD spectrum even if it is weak in the optical absorption spectrum.

The good agreement between the bare cluster calculations and our data, in both overall spectral shapes and peak intensities, suggests that the low-energy experimental CD may be dominated by free electron transitions of a chiral, filamentary cluster. The positive, monosignate CD that overlies the primary absorbance resonance (Figure 4) arises from the filamentary cluster shape and is in marked contrast to the bisignate CD characteristic of quasi-spherical metal nanoparticles with chiral shape distortions.[36]

An alternative mechanism that has been calculated[37] and observed[38−40] for much larger metal nanoparticles is induced CD (ICD) at the plasmon energy, arising from nonresonant Coulomb coupling to the UV transitions of chiral molecules. This produces a monosignate CD peak overlying the plasmon absorbance. The ICD sign can be negative or positive, depending on the orientation of the chiral molecule relative to the nanoparticle surface, and the magnitude is proportional to the number of metal atoms and inversely proportional to the cube of the separation between the metal particle and the chiral molecule. While size scaling suggests that such an effect may be weak in the cluster regime,[41] the theory was developed for much larger particles without discrete transitions, for which the chiral molecules could be treated as point-like. (We also note that molecular mechanisms for nonresonant ICD can produce a monosignate ICD signal at the absorbance transitions of small, achiral molecules bound in the DNA groove,[42] with sign and magnitude dependent on the relative orientation of the groove binder and DNA.) Although the main features in the low-energy, cluster-dominated CD of Ag_N-DNA are captured by a chiral, filamentary Ag cluster, ICD may also contribute in our experiments.

Solvent-Driven Conformational Shift. For sample S4, the blue-green fluorescent Ag_N-DNA, we found that changes in solvent composition alone could induce dramatic changes in both absorbance and CD spectra that are indicative of a solvent-mediated equilibrium between two distinct species: a fluorescent silver cluster and a conformationally distinct, nonfluorescent form. In aqueous solution, the pure S4 Ag_N-DNA absorbance spectrum shows low-energy peaks at both 2.54 and 3.04 eV, with the higher energy peak more intense (blue curve, Figure 5b). Increasing methanol concentration strengthens the 2.54 eV absorbance and weakens the 3.04 eV absorbance peak, which can no longer be detected at 50% methanol by volume (black curve, Figure 5b). The fluorescence excitation spectra (Figure 5c), measured by detecting at the peak emission energy (2.19 eV) while scanning the excitation wavelength, show that only the 2.54 eV absorbing form

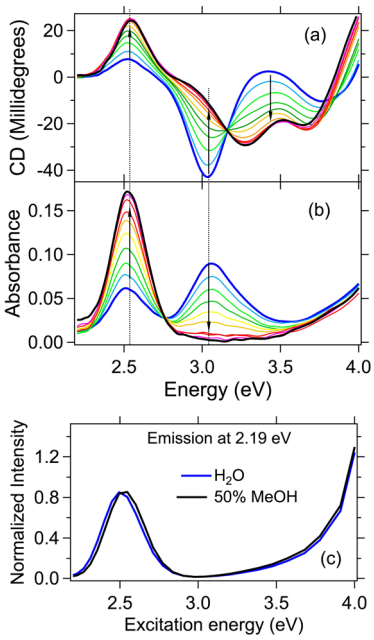

Figure 5. (a) CD and (b) absorbance spectra for the titration of sample S4 from 0 to 50% methanol by volume in 5% increments. Direction of arrows indicates increasing methanol concentration. (c) Fluorescence excitation spectrum of sample S4 in water and in 50% methanol. Detection at emission peak (2.19 eV).

is fluorescent. A dramatic increase in fluorescence intensity with increasing methanol fraction (a factor of 5 at 50% methanol, relative to aqueous solution) accompanies the disappearance of the 3.04 eV absorbance peak, again confirming that it is associated with a nonfluorescent form.

These solvent-driven changes in optical spectra are reversible, as determined by use of spin filtration to change solvent composition while retaining the DNA. Cycling the solvent between 0% and 50% MeOH shifted the absorbance spectra between the blue (0% MeOH) and black (50% MeOH) traces in Figure 5b. Silver cations or small clusters released into the solvent would be removed by filtration and produce irreversible changes, contrary to the reversible behavior we find. Thus, overall silver content is conserved between fluorescent and dark forms. The well-defined isodichroic point at 3.16 eV (Figure 5a) further indicates an equilibrium between two distinct species having the same overall silver content but different structure.

Apparently the titration of S4 with methanol produces structural changes that strongly influence electronic structure. Increasing methanol concentration favors the fluorescent form, with dichroic bands similar to the other pure, fluorescent Ag_N-DNA in aqueous solution. Titration with sucrose, rather than methanol, produces similar enhancement of the fluorescent form. Apparently solvent composition can be manipulated to activate the DNA structural motifs most conducive to the structure that maximizes fluorescence quantum yield.

Since higher transition energies correspond to shorter silver cluster chains,[15] changes in Ag−Ag bonding may be responsible for the 0.5 eV increase in peak absorbance energy between the fluorescent and dark forms, which have significantly different CD spectra. The fluorescent form has a positive CD peak that overlies the main cluster absorbance peak (Figure 5a,b, black curves), the same as for the other fluorescent clusters. In contrast, the dark form exhibits a negative dichroic peak near the 3.04 eV absorbance maximum and a pronounced positive shift in CD amplitude at higher energy (Figure 5ab, blue curves).

An equilibrium between dark and fluorescent forms of silver-decorated DNA with different absorbance energies and the same total silver content was found previously in studies of the hybridization of complementary strands to silver-bearing DNA.[43] Thus, changes in the DNA environment can produce similar behavior to altering solvent composition.

The addition of alcohols and sucrose as cosolvents is known to alter DNA conformation through changes in hydration.[44,45] Thus, it appears that cosolvent-mediated alterations of DNA conformation induce structural changes in the embedded silver clusters.

CONCLUSIONS

The chiral structure of four different species of pure Ag_N-DNA has been investigated using circular dichroism and absorbance spectroscopy and compared to quantum chemical calculations for bare silver cluster chains with nonplanar curvature. In all cases, the data show a monosignate, positive CD peak that overlies the lowest energy absorbance transition and highly anisotropic, negative dichroic peaks well below the UV transitions of the bases. Thus, despite their different colors, all of the DNA-stabilized silver clusters studied here appear to belong to the same structural family. Agreement in spectral shapes and overall CD magnitudes between experiment and theory suggests that helical, filamentary silver clusters are present experimentally.

In the UV, the similar CD structure across all pure Ag_N-DNA and the much higher CD amplitudes than for the bare strands indicate that nucleobases near the clusters are held in similar, compacted geometries. The smallest cluster, S4, exhibits a solvent-tuned equilibrium between fluorescent and dark conformations, suggesting new sensing possibilities for solvent-induced changes in the immediate environment of the cluster. Our work provides a new perspective on chirality of ligand-protected metal clusters, in an entirely different size regime from the many previous studies of chirality in much larger metal nanoparticles and nanoparticle assemblies. These studies of silver clusters make possible a more transparent connection between CD

spectra and cluster structure than for their more frequently studied gold cluster counterparts, due to the larger energetic separation of localized d orbitals from delocalized cluster states.

MATERIALS AND METHODS

Synthesis and Purification of Ag_N-DNA. DNA oligomers were obtained from Integrated DNA Technologies with standard desalting. All solutions, except HPLC running buffers, were made with RNase/DNase-free distilled water from Life Technologies. All other chemicals used were analytical grade or higher. DNA strands were selected from previously reported sequences known to form silver cluster emitters of varying wavelengths.[18,21,22,46] The Ag_N-DNAs were synthesized by annealing solutions of bare DNA oligomers in 7.5 mM ammonium acetate buffer with optimized silver nitrate (75−250 μM) and DNA (5−20 μM) concentrations at 90 °C for 5 min and allowing them to cool slowly to ambient temperature. Solutions were reduced with sodium borohydride in a ratio of half that to silver nitrate and allowed to react in optimized temperature (4−40 °C) conditions for each sample.

Samples were purified using reverse-phase high-performance liquid chromatography (HPLC), with water−methanol solvent mixtures in 35 mM triethylamine acetate (TEAA) as the ion-pairing agent to the C_{18} column (Phenomenex). The gradient was optimized for each sample and in each case started between 5% and 20% methanol by volume and ended between 20% and 40% methanol, with a 1% per minute gradient. To estimate purity, we compared absorbance chromatograms measured at the peak visible excitation wavelength of the fluorescent Ag_N-DNA to the 260 nm absorbance chromatograms, which provided a conservative estimate of 80% purity in all samples. Following collection of the pure samples, they were solvent exchanged back to 7.5 mM ammonium acetate by spin filtration, which ensured that less than 0.5% of the running buffer remained.

Optical Characterization. All absorption and fluorescence spectra were measured using a thermoelectrically cooled array detector (Ocean Optics QE65000). The CD data were collected using a circular dichrometer (Aviv 202) at ambient temperature. The instrument's wavelength accuracy was calibrated with a 40 g/L holmium oxide in 10% perchloric acid standard solution (Agilent Technologies). The samples were run at concentrations required to reach the ideal 0.87 absorbance for dichroic measurements.[47] Purified S2 did not achieve this ideal absorbance due to low chemical yields; however it was still within allowable analytical range. Blanks with appropriate concentrations of buffer were run before and after each sample and averaged for the blank subtraction. The spectra were normalized to molar ellipticity by their absorbances at 4.77 eV (260 nm) using the nearest neighbor calculated molar extinction coefficients for the DNA oligomers.

For methanol titrations of sample S4, a blank with pure water was taken before the titration and a blank with 50% methanol was taken after the titration. The data were corrected by applying a linear background subtraction to account for drift, and the data were corrected for the DNA concentration dilution from added methanol. The solution equilibrated for 20 min after each addition of methanol before collecting the spectra. This was shown to be sufficient time by conducting a titration while monitoring fluorescence intensities.

Calculation Techniques. The Amsterdam Density Functional (ADF) program[48] was used for calculation of optical absorption and circular dichroism spectra. In the ADF calculations, scalar relativistic effects are included by utilizing the zero-order regular approximation (ZORA).[49] Time-dependent density functional theory (TDDFT) is employed to calculate excited states. For these calculations we used the asymptotically correct SAOP functional.[50] This functional was combined with a triple-ζ plus polarization (TZP) Slater-type basis set. The SCF convergence is tightened to 10^{-8}, the tolerance was set to 10^{-8}, and the orthonormality was set to 10^{-10}. The first 200 dipole-allowed transitions were evaluated for the optical absorption and CD spectrum.

The simulation of the CD spectra is based on the relations[3,51,52]

$$\Delta\varepsilon = 4\alpha \sum_m R_m E_m \sigma_m(E)$$

$$\alpha = \frac{4\pi N_A}{3\ln(10)10^3}\frac{2\pi}{hc}$$

$$\sigma_m(E) = \frac{1}{\sigma\sqrt{2\pi}}\exp\left(-\frac{1}{2\sigma^2}(E - E_m)^2\right)$$

where $\Delta\varepsilon$ is molar circular dichroism or molar differential dichroic absorptivity in units of $L\cdot mol^{-1}\cdot cm^{-1}$, α is a set of constants, N_A is Avogadro's number in units of mol^{-1}, h is the Planck constant in units of J·s, c is the speed light in units of cm/s, R_m is rotatory strength in units of $esu^2\cdot cm^2$, E is the energy of the incident light in eV, E_m is the excitation energy to state M in eV, $\sigma_m(E)$ is the Gaussian band shape factor, and σ is the exponential half-width (we used σ = 0.2 eV). Molar circular dichroism is related to molar ellipticity by the following equation:[53]

$$[\Theta] = 3298 \times 2\Delta\varepsilon$$

where $[\Theta]$ is molar ellipticity, expressed in $deg\cdot cm^2\cdot dmol^{-1}$.

Conflict of Interest: The authors declare no competing financial interest.

Acknowledgment. This work was supported by NSF-CHE-1213895 and NSF-CHE-1213771. We thank Kevin Plaxco for informative discussions.

Supporting Information Available: Synthesis and purification parameters for each Ag_N-DNA; purity estimates and associated absorbance chromatograms; additional information on quantum chemical calculations; comparison of pure and impure CD spectra. This material is available free of charge *via* the Internet at http://pubs.acs.org.

REFERENCES AND NOTES

1. Lu, F.; Tian, Y.; Liu, M.; Su, D.; Zhang, H.; Govorov, A. O.; Gang, O. Discrete Nanocubes as Plasmonic Reporters of Molecular Chirality. *Nano Lett.* **2013**, *13*, 3145–3151.
2. Farrag, M.; Tschurl, M.; Heiz, U. Chiral Gold and Silver Nanoclusters: Preparation, Size Selection, and Chiroptical Properties. *Chem. Mater.* **2013**, *25*, 862–870.
3. Lopez-Acevedo, O.; Tsunoyama, H.; Tsukuda, T. Chirality and Electronic Structure of the Thiolate-Protected Au38 Nanocluster. *J. Am. Chem. Soc.* **2010**, *132*, 8210–8218.
4. Knoppe, S.; Dolamic, I.; Bürgi, T. Racemization of a Chiral Nanoparticle Evidences the Flexibility of the Gold-Thiolate Interface. *J. Am. Chem. Soc.* **2012**, *134*, 13114–13120.
5. Dolamic, I.; Knoppe, S.; Dass, A.; Bürgi, T. First Enantioseparation and Circular Dichroism Spectra of Au38 Clusters Protected by Achiral Ligands. *Nat. Commun.* **2012**, *3*, 798.
6. Ravindran, A.; Chandran, P.; Khan, S. S. Biofunctionalized Silver Nanoparticles: Advances and Prospects. *Colloids Surf. B: Biointerfaces* **2013**, *105*, 342–352.
7. Kuzyk, A.; Schreiber, R.; Fan, Z.; Pardatscher, G.; Roller, E.; Högele, A.; Simmel, F. C.; Govorov, A. O.; Liedl, T. DNA-Based Self-Assembly of Chiral Plasmonic Nanostructures with Tailored Optical Response. *Nature* **2012**, *483*, 311–314.
8. Chandra, M.; Dowgiallo, A.-M.; Knappenberger, K. L. Magnetic Dipolar Interactions in Solid Gold Nanosphere Dimers. *J. Am. Chem. Soc.* **2012**, *134*, 4477–4480.

9. Caro, C.; Castillo, P. M.; Klippstein, R.; Pozo, D.; Zaderenko, A. P. Silver Nanoparticles: Sensing and Imaging Applications. In *Silver Nanoparticles*; Perez, D. P., Ed.; InTech, 2010; pp 202−223.
10. Latorre, A.; Somoza, Á. DNA-Mediated Silver Nanoclusters: Synthesis, Properties and Applications. *ChemBioChem* **2012**, *13*, 951–958.
11. Han, B.; Wang, E. DNA-Templated Fluorescent Silver Nanoclusters. *Anal. Bioanal. Chem.* **2012**, *402*, 129–138.
12. Udayabhaskararao, T.; Pradeep, T. New Protocols for the Synthesis of Stable Ag and Au Nanocluster Molecules. *J. Phys. Chem. Lett.* **2013**, *4*, 1553–1564.
13. Aikens, C. M. Electronic Structure of Ligand-Passivated Gold and Silver Nanoclusters. *J. Phys. Chem. Lett.* **2011**, *2*, 99–104.
14. Johnson, H. E.; Aikens, C. M. Electronic Structure and TDDFT Optical Absorption Spectra of Silver Nanorods. *J. Phys. Chem. A* **2009**, *113*, 4445–4450.
15. Guidez, E. B.; Aikens, C. M. Theoretical Analysis of the Optical Excitation Spectra of Silver and Gold Nanowires. *Nanoscale* **2012**, *4*, 4190–4198.
16. Yan, J.; Gao, S. Plasmon Resonances in Linear Atomic Chains: Free-Electron Behavior and Anisotropic Screening of D Electrons. *Phys. Rev. B* **2008**, *78*, 235413.
17. Petty, J. T.; Fan, C.; Story, S. P.; Sengupta, B.; John, A. S.; Prudowsky, Z.; Dickson, R. M. DNA Encapsulation of Ten Silver Atoms. *J. Phys. Chem. Lett.* **2011**, *1*, 2524–2529.
18. Schultz, D.; Gwinn, E. G. Silver Atom and Strand Numbers in Fluorescent and Dark Ag:DNAs. *Chem. Commun. (Cambridge, UK)* **2012**, *48*, 5748–5750.
19. Schultz, D.; Gardner, K.; Oemrawsingh, S. S. R.; Markešević, N.; Olsson, K.; Debord, M.; Bouwmeester, D.; Gwinn, E. Evidence for Rod-Shaped DNA-Stabilized Silver Nanocluster Emitters. *Adv. Mater.* **2013**, *25*, 2797–2803.
20. Copp, S. M.; Schultz, D.; Swasey, S.; Pavlovich, J.; Debord, M.; Chiu, A.; Olsson, K.; Gwinn, E. Magic Numbers in DNA-Stabilized Fluorescent Silver Clusters Lead to Magic Colors. *J. Phys. Chem. Lett.* **2014**, *5*, 959–963.
21. Neidig, M. L.; Sharma, J.; Yeh, H.; Martinez, J. S.; Conradson, S. D.; Shreve, A. P. Ag K-Edge EXAFS Analysis of DNA-Templated Fluorescent Silver by DNA Sequence Variations. *J. Am. Chem. Soc.* **2011**, *133*, 11837–11839.
22. Petty, J. T.; Fan, C.; Story, S. P.; Sengupta, B.; Sartin, M.; Hsiang, J.; Perry, J. W.; Dickson, R. M. Optically Enhanced, near-IR, Silver Cluster Emission Altered by Single Base Changes in the DNA Template. *J. Phys. Chem. B* **2011**, *115*, 7996–8003.
23. Sharma, J.; Rocha, R. C.; Phipps, M. L.; Yeh, H.; Balatsky, K. A.; Vu, D. M.; Shreve, A. P.; Werner, J. H.; Martinez, J. S. A DNA-Templated Fluorescent Silver Nanocluster with Enhanced Stability. *Nanoscale* **2012**, *4*, 4107–4110.
24. Lan, G.; Chen, W.; Chang, H. One-Pot Synthesis of Fluorescent Oligonucleotide Ag Nanoclusters for Specific and Sensitive Detection of DNA. *Biosens. Bioelectron.* **2011**, *26*, 2431–2435.
25. Petty, J. T.; Zheng, J.; Hud, N. V.; Dickson, R. M. DNA-Templated Ag Nanocluster Formation. *J. Am. Chem. Soc.* **2004**, *126*, 5207–5212.
26. Kypr, J.; Kejnovská, I.; Renciuk, D.; Vorlícková, M. Circular Dichroism and Conformational Polymorphism of DNA. *Nucleic Acids Res.* **2009**, *37*, 1713–1725.
27. Edwards, E. L.; Ratliff, R. L.; Gray, D. M. Circular Dichroism Spectra of DNA Oligomers Show That Short Interior Stretches of C.C+ Base Pairs Do Not Form in Duplexes with A.T Base Pairs. *Biochemistry* **1988**, *27*, 5166–5174.
28. Studdert, D. S.; Patroni, M.; Davis, R. C. Circular Dichroism of DNA: Temperature and Salt Dependence. *Biopolymers* **1972**, *11*, 761–779.
29. Ono, A.; Cao, S.; Togashi, H.; Tashiro, M.; Fujimoto, T.; Machinami, T.; Oda, S.; Miyake, Y.; Okamoto, I.; Tanaka, Y. Specific Interactions between silver(I) Ions and Cytosine-Cytosine Pairs in DNA Duplexes. *Chem. Commun. (Cambridge, UK)* **2008**, 4825–4827.
30. Nordén, B.; Matsuoka, Y.; Kurucsev, T. Nucleic Acid-Metal Interactions: V. The Effect of Silver(I) on the Structures of A- and B-DNA Forms. *Biopolymers* **1986**, *25*, 1531–1545.
31. Menzer, S.; Sabat, M.; Lippert, B. Ag (I) Modified Base Pairs Involving Complementary (G, C) and Noncomplementary (A, C) Nucleobases. on the Possible Structural Role of Aqua Ligands in Metal-Modified Nucleobase Pairs. *J. Am. Chem. Soc.* **1992**, *114*, 4644–4649.
32. Zavriev, S. K.; Minchenkova, L. E.; Vorlickova, M.; Kolchinsky, A. M.; Volkenstein, M. W.; Ivanov, V. I. Circular Dichroism Anisotropy of DNA with Different Modifications at N7 of Guanine. *Biochim. Biophys. Acta* **1979**, *564*, 212–224.
33. Berova, N.; Di Bari, L.; Pescitelli, G. Application of Electronic Circular Dichroism in Configurational and Conformational Analysis of Organic Compounds. *Chem. Soc. Rev.* **2007**, *36*, 914–931.
34. O'Neill, P. R.; Gwinn, E. G.; Fygenson, D. K. UV Excitation of DNA Stabilized Ag Cluster Fluorescence *via* the DNA Bases. *J. Phys. Chem. C* **2011**, *115*, 24061–24066.
35. Ramazanov, R. R.; Kononov, A. I. Excitation Spectra Argue for Threadlike Shape of DNA-Stabilized Silver Fluorescent Clusters. *J. Phys. Chem. C* **2013**, *117*, 18681–18687.
36. Fan, Z.; Govorov, A. O. Chiral Nanocrystals: Plasmonic Spectra and Circular Dichroism. *Nano Lett.* **2012**, *12*, 3283–3289.
37. Govorov, A. O. Plasmon-Induced Circular Dichroism of a Chiral Molecule in the Vicinity of Metal Nanocrystals. Application to Various Geometries. *J. Phys. Chem. C* **2011**, *115*, 7914–7923.
38. Maoz, B. M.; van der Weegen, R.; Fan, Z.; Govorov, A. O.; Ellestad, G.; Berova, N.; Meijer, E. W.; Markovich, G. Plasmonic Chiroptical Response of Silver Nanoparticles Interacting with Chiral Supramolecular Assemblies. *J. Am. Chem. Soc.* **2012**, *134*, 17807–17813.
39. Maoz, B.; Chaikin, Y.; Tesler, A.; Elli, O. B. Amplification of Chiroptical Activity of Chiral Biomolecules by Surface Plasmons. *Nano Lett.* **2013**, *13*, 1203–1209.
40. Li, Z.; Zhu, Z.; Liu, W.; Zhou, Y.; Han, B. Reversible Plasmonic Circular Dichroism of Au Nanorod and DNA Assemblies. *J. Am. Chem. Soc.* **2012**, *134*, 3322–3325.
41. Govorov, A. O.; Fan, Z.; Hernandez, P.; Slocik, J. M.; Naik, R. R. Theory of Circular Dichroism of Nanomaterials Comprising Chiral Molecules and Nanocrystals: Plasmon Enhancement, Dipole Interactions, and Dielectric Effects. *Nano Lett.* **2010**, *10*, 1374–1382.
42. Nordén, B.; Kurucsev, T. Analysing DNA Complexes by Circular and Linear Dichroism. *J. Mol. Recognit.* **1994**, *7*, 141–155.
43. Petty, J. T.; Sergev, O. O.; Nicholson, D. A.; Goodwin, P. M.; Giri, B.; McMullan, D. R. A Silver Cluster-DNA Equilibrium. *Anal. Chem.* **2013**, *85*, 9868–9876.
44. Spink, C. H.; Garbett, N.; Chaires, J. B. Enthalpies of DNA Melting in the Presence of Osmolytes. *Biophys. Chem.* **2007**, *126*, 176–185.
45. Son, I.; Shek, Y. L.; Dubins, D. N.; Chalikian, T. V. Hydration Changes Accompanying Helix-to-Coil DNA Transitions. *J. Am. Chem. Soc.* **2014**, *136*, 4040–4047.
46. Schultz, D.; Copp, S. M.; Markešević, N.; Gardner, K.; Oemrawsingh, S. S. R.; Bouwmeester, D.; Gwinn, E. Dual-Color Nanoscale Assemblies of Structurally Stable, Few-Atom Silver Clusters, As Reported by Fluorescence Resonance Energy Transfer. *ACS Nano* **2013**, *7*, 9798–9807.
47. Bishop, G. R.; Chaires, J. B. Characterization of DNA Structures by Circular Dichroism. *Curr. Protoc. Nucleic Acid Chem.* **2003**, *11*, 7.11.1–7.11.8.
48. Te Velde, G.; Bickelhaupt, F. M.; Baerends, E. J.; Fonseca Guerra, C.; van Gisbergen, S. J. A.; Snijders, J. G.; Ziegler, T. Chemistry with ADF. *J. Comput. Chem.* **2001**, *22*, 931–967.
49. Van Lenthe, E.; van Leeuwen, R.; Baerends, E. J.; Snijders, J. G. Relativistic Regular Two-Component Hamiltonians. *Int. J. Quantum Chem.* **1994**, *57*, 281–293.
50. Schipper, P. R. T.; Grittsenko, O. V.; van Gisbergen, S. J. A.; Baerends, E. J. Molecular Calculations of Excitation Energies and (Hyper) Polarizabilities with a Statistical Average of Orbital Model Exchange-Correlation Potentials. *J. Chem. Phys.* **2000**, *112*, 1344–1352.
51. Autschbach, J.; Ziegler, T.; van Gisbergen, S. J. A.; Baerends, E. J. Chiroptical Properties from Time-Dependent Density

Functional Theory. I. Circular Dichroism Spectra of Organic Molecules. *J. Chem. Phys.* **2002**, *116*, 6930.
52. Crawford, T. D. Ab Initio Calculation of Molecular Chiroptical Properties. *Theor. Chem. Acc.* **2005**, *115*, 227–245.
53. Woody, R. Circular Dichroism. *Methods Enzymol.* **1995**, *246*, 34–71.